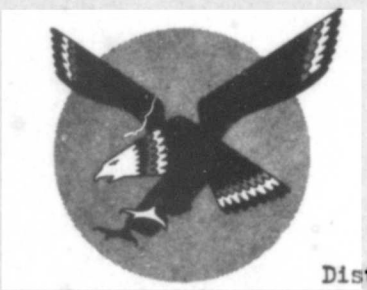

Distribution of this document is unlimited.

CONVAIR

A DIVISION OF GENERAL DYNAMICS CORPORATION
SAN DIEGO

CONVAIR

A DIVISION OF GENERAL DYNAMICS CORPORATION

SAN DIEGO

REPORT RT 60-106

DATE 10 March 1961

MODEL 7

TITLE

HEAT TRANSFER RATES IN THE VICINITY OF SURFACE PROTUBERANCES AT MACH 6.3

Distribution of this document is unlimited.

PREPARED BY F.P. Baltakis

F.P. Baltakis

Checked by P.P. Lee

P.P. Lee

CHECKED BY R.F. Holmes

R.F. Holmes

GROUP Thermodynamics Laboratories

REFERENCE

APPROVED BY W.L. Dittmann

W.L. Dittmann

Chief, Thermodynamics Laboratories

NO. OF PAGES

NO. OF DIAGRAMS

REVISIONS

NO.	DATE	BY	CHANGE	PAGES AFFECTED

FORM 1812 A-4

I

SUMMARY

Wind tunnel tests were conducted to determine the effects of various protuberances on heat transfer rates to a flat surface. The protuberance models included three cylinders inclined 45 degrees backward, two cylinders inclined 45 degrees forward, two cylinders normal to the flow, one semi-cone-afterbody and one wedge-afterbody model. Tests were performed at Mach 6.3 and at gas total temperature of 4350 °R.

The degree and the lateral extent of disturbances produced by cylindrical protuberances depend on the protuberance orientation with respect to the flow. Models inclined forward produced the highest heating rates while models inclined backward produced the lowest.

Cylindrical protuberances inclined 45 degrees backward produced no significant increase in heating rates upstream of the models. Models in normal or forward facing orientation produced an increased heating rate area that extends approximately 2-1/2 protuberance diameters upstream.

The highest heating rate region in the vicinity of cylindrical protuberances inclined 45 degrees backward occurred along the lines that are trailing the models at approximately 10 degrees with respect to the plate centerline. Cylindrical protuberances in normal and forward-facing attitudes produced the highest heating rates just upstream of the models.

Downstream and to the sides of the cylindrical protuberances disturbances extended throughout the instrumented length.

The highest heating rates, about 40 times the undisturbed value, occurred upstream of the forward-facing cylindrical protuberances.

INTRODUCTION

Convective heat transfer rates on a surface exposed to a supersonic flow may be significantly altered by a surface protuberance. The degree and the lateral extent of disturbances appear to depend on protuberance geometry, free stream conditions, and condition of the boundary layer.

Interaction of protuberance shock waves with the boundary layer produces a flow field which at present cannot be adequately treated analytically. Experimental studies have been initiated and data is available for a number of specific protuberance configurations (References 1 through 7). As at present, however, experimental investigations have included only a small percentage of the protuberance configurations of

INTRODUCTION (Cont'd)

interest. The available data is still insufficient for establishment of semi-empirical relations for heat transfer or flow parameters in the disturbed regions.

The purpose of this investigation was to provide additional experimental heat transfer data for protuberance configurations that are of interest in current missile design. The rocket-powered wind tunnel, available for this investigation, provided a test environment that closely simulates typical missile flight conditions.

TEST APPARATUS

The heat transfer surveys were conducted in the Thermodynamics Laboratories' rocket powered wind tunnel. The tunnel working fluid was generated by burning gaseous hydrogen and air at a stoichiometric mixture ratio at 465 psia chamber pressure. A supersonic test jet was obtained by expanding the combustion products through an axi-symmetric reflex nozzle.

The test section flow parameters are given in Table I. The method used to obtain these parameters is described in the Appendix. The combustion chamber properties and gas composition are given in Table II.

The heat transfer surveys were made utilizing a plate with one surface flat and parallel to the free stream. A twenty-degree copper wedge was attached at the leading edge to secure a flow of minimum disturbance over the instrumented surface. Installation of the plate in the tunnel is shown in Figure 1. Details of construction are shown in Figure 2.

The protuberance models included three cylinders of 0.75, 1.0, and 1.5 inches diameter, a semi-cone with an afterbody, and a 30-degree wedge with an after-body. The two smaller diameter cylindrical models were tested at three different attitudes with respect to the flow: 1) normal, 2) inclined 45-degrees forward, and 3) inclined 45-degrees baskward. Because of excessive wind tunnel blockage the 1.5 inches diameter model could not be tested in normal or forward attitudes.

The base plate was instrumented with 59 thermocouples and three static pressure orifices. The thermocouples were spot-welded to the back side of the surface plate. Arrangement of the thermocouples and pressure orifices is seen in Figure 6. The cylindrical protuberance models were instrumented with thermocouples using the spot-welding technique. The semi-cone and wedge-afterbody models were instrumented with plug-type copper calorimeters. Locations of the instrumented points on the protuberance models are shown in Figures 3, 4, and 5.

TEST APPARATUS (Cont'd)

The condition of the boundary layer over the protuberance-free surface was examined by comparing the measured heating rates to the rates calculated for laminar and turbulent boundary layers. The theoretical values were obtained using the reference enthalpy method suggested by Eckert in Reference 8. As seen in Figure 18, better agreement with experimental values was obtained using theoretical laminar values rather than theoretical turbulent values.

DATA REDUCTION

The rate of heat transfer to the exposed surface was determined from the following equation:

$$q = q_s + q_c + q_r$$

The left hand term represents the heat transfer rate received by a surface element from the hot gas stream; q_s is the rate at which the energy is stored in the element; q_c is the net rate at which the heat is conducted laterally to or from the element; and q_r is the rate at which the heat is radiated through the back surface. The radiation loss through the back surface of the skin was estimated to be less than 2% of the total at the maximum temperature measured. The lateral conduction loss depends on the second temperature-lateral distance derivative. To determine this correction using the temperature derivative method an accurate temperature distribution in the lateral plane is necessary. In the vicinity of protuberance models, where the variation in temperature gradients is large and rapidly changing, the temperature distribution was not known accurately enough to determine the second temperature-distance derivative. As an alternate approach the following method was used to obtain the lateral conduction losses.

The high total temperature environment provided a very nearly constant skin temperatur. rise rate. Therefore, at points which were free of conduction losses the temperature-time traces were very nearly straight lines. Points with conductive heat losses produced traces deviating from a straight line. After the tunnel shut-off the temperatures at these points continued to rise or fall depending on whether the net conductive heat transfer was positive or negative. The correction for the lateral conduction was determined by measuring the temperature-time gradient immediately after shut-off of the tunnel flow.

The aerodynamic heating rates on the surface plate was then obtained from the equation:

$$q = d \cdot \rho \cdot C_p \frac{\partial T}{\partial t}$$

DATA REDUCTION (Cont'd)

where d is thickness of the skin, ρ density of the skin, C_p - specific heat of the skin, and $\frac{\Delta T}{\Delta t}$ - measured temperature gradient corrected for losses.

The aerodynamic heating rates on the cylindrical protuberances were obtained from a similar equation:

$$q = \frac{2 R_1}{R_1 + R_2} \cdot d \cdot \rho \cdot C_p \frac{\Delta T}{\Delta t}$$

where $\frac{2 R_1}{R_1 + R_2}$ is a curvature correction factor introduced to account for increased area of the exposed convex surface. The lateral conduction effects were corrected in the same manner as for the base plate surface. The semi-cone and wedge-afterbody models were equipped with plug-type calorimeters. The heating rates were calculated from equation:

$$q = d \cdot \rho \cdot C_p \cdot \frac{\Delta T}{\Delta t}$$

Where d, ρ, and C_p are the length, density, and specific heat of the calorimeter and $\Delta T/\Delta t$ the measured temperature rise rate.

RESULTS AND DISCUSSION

Method of Presentation:

Heat transfer rates to the base plate in the vicinity of the protuberances are given in Figures 7 through 15. To indicate the protuberance effects the data are presented in the form of ratios of local disturbed to undisturbed (protuberance-free) heat transfer rates. The flat plate undisturbed heat transfer rates are given in Table III. The heat transfer rates on the protuberance models are given in Figures 16 and 17.

Undisturbed Flat Plate

The undisturbed flat plate heat transfer rates were averaged for three or more runs and are presented in Table III. The data were taken along the centerline and along lines parallel to and 0.75 and 1.5 inches away from the centerline. The agreement among the corresponding values on these three lines is considered satisfactory. A more pronounced devi-

RESULTS AND DISCUSSION (Cont'd)

ation of the farthest measurements near the trailing end is probably due to the edge effects. Variation along the centerline is shown in Figure 18. The heat transfer rates measured on the upstream half of the plate closely approach a parabolic distribution. On the downstream half of the plate the distribution is less regular but the values fall in the vicinity of the same parabolic curve.

Cylindrical Protuberances Inclined 45° Backward

Protuberance effects on heat transfer rates to the flat plate are shown in Figures 7, 8, and 9. The heating rates near the leading edge are about 20% higher than the undisturbed values. The rates decrease gradually to approximately 80% of the undisturbed rates about one protuberance radius upstream of the models. Just upstream of the models the rates increase to approximately the undisturbed values. Downstream close to the models the heating rates are less than 30% of the undisturbed values. About 4 diameters downstream the rates increase to approximately 3 times the undisturbed values. To the sides the hottest regions trail the models at approximately 10° angle with respect to the plate centerline. In the area surveyed the highest rates occurred farthest away from the models.

The maximum heating rates increased with the size of the model. The highest obtained with 1.5 inches diameter model is 8.37 times the undisturbed value.

Cylindrical Protuberances Normal to the Flow

As seen in Figures 10 and 11 increased heating area extends approximately 2-1/2 diameters upstream of the protuberance. The heating rates in this region undergo the following variation: 1) an increase to approximately 3 times the undisturbed value, 2) a decrease to approximately 1.4 times the undisturbed value, and 3) a very pronounced increase just upstream of the model. The highest values measured upstream of the 3/4 and 1-inch diameter models were 31.8 and 10.3 times the undisturbed values. The difference in these measurements is probably due to dissimilarity in the instrumentation arrangement with respect to the flow fields for the two models.

Downstream close to the models the rates are below the undisturbed values. About 2 diameters downstream the rates peak at approximately 4 times and 3 times the undisturbed values for the 3/4 and 1-inch diameter models respectively. To the sides the hottest regions trail the models at approximately 20-degrees with respect to the plate centerline. The highest rates

RESULTS AND DISCUSSION (Cont'd)

recorded in these regions for the 3/4 and 1-inch diameter models were 12.0 and 11.45 times the undisturbed value.

Cylindrical Protuberances Inclined 45° Forward

Heat transfer rates to the base plate are given in Figures 12 and 13. Increased heating rates extend approximately 2-1/2 protuberance diameters upstream. The maximum rates, approximately 40 times the undisturbed value, occurred less than 1/2 protuberance diameters upstream of both models. Directly downstream of the models heating rates are higher than for the same models oriented normal to the flow. To the sides near the models the heating rates are higher than for the same models normal to the flow. The rates farther away are somewhat lower than for normal cylinders. An increase-decrease-increase pattern in the direction of the flow occurred as in the cases of normal and 45°-backward orientations.

Semi-cone-Afterbody Protuberance

In the close vicinity upstream and downstream of the model the heating rates are approximately 50% of the undisturbed values. Farther downstream the rate increased to 1.36 times the undisturbed value. The highest heating rate, 2.66 times the undisturbed value, occurred to the side and downstream of the model.

Wedge-Afterbody Protuberance

As seen in Figure 15 the heating rate about one protuberance thickness upstream of the model is approximately 50% of the undisturbed value. Downstream, close to the model, the rate is less than 20% of the undisturbed value. Farther downstream the rates increase gradually to 2.29 times the undisturbed values.

Heat Transfer Rates to Protuberance Models

The heating rates to the cylindrical protuberance models are shown in Figure 16. On protuberances inclined backward the peak in distribution along the leading edge occurred 1/4-inch above the surface of the base plate. On protuberances in normal orientation the peak occurred 3/4-inch above the surface. On protuberances inclined forward one peak occurred very close to the surface and the second peak approximately 1/2-inch above the surface. The peak rates as well as the overall heat transfer rates were highest on smallest diameter protuberances.

RESULTS AND DISCUSSION (Cont'd)

The heating rates on semi-cone and wedge-afterbody protuberance models are shown in Figure 17. The highest heating rates were measured nearest to the leading edges on both models. At the trailing ends the rates dropped to 6% and 16% of the respective highest measured values on the semi-cone and wedge-afterbody protuberances. The highest rate on the semi-cone model was nearly four times the highest measured rate on the wedge-afterbody model.

CONCLUSIONS

The degree and the lateral extent of disturbances produced by cylindrical protuberances depend on the model orientation with respect to the flow. Models inclined forward produced the highest heating rates while models inclined backward produced the lowest.

Cylindrical models inclined 45° backward produced no significant increase in heating rates upstream of the models. Models in normal or forward-facing orientation produced an increased heating rate area that extends approximately 2.5 protuberance diameters upstream.

The highest heating rate region in the vicinity of cylindrical models inclined 45° backward occurred along the lines that are trailing the models at approximately 10 degrees with respect to the plate centerline. Cylindrical protuberances in normal or forward-facing attitudes produced the highest heating rates just upstream of the models.

Downstream and to the sides of the cylindrical models disturbances extended throughout the instrumented length.

The highest heating rates, about 40 times the undisturbed value, occurred upstream of the forward-facing cylindrical protuberances.

APPENDIX

Determination of Test Section Flow Properties

The test section flow properties were determined analytically and were checked using calibration pressure and massflow data. In the calculations the expansion process was assumed to take place at a shifting gas composition from combustion chamber pressure to 25 psia and at a frozen gas composition from 25 psia pressure to the test section static pressure. As shown in Reference 9 the vibrational relaxation time for nitrogen-water vapor mixture is very short. The vibrational relaxation time at the test section static conditions is of the order of 30 microseconds and is considerably less at higher pressures and temperatures. The nozzle travel time is approximately 300 microseconds. The gases, therefore, were assumed to be in a thermodynamic equilibrium throughout the expansion process. The calculations for test section velocity, static temperature, and Mach number were carried out using a step expansion method. The measured test section static pressure was taken as the lower limit for the expansion process.

The combustion chamber gas temperature and the test section total temperature were considered to be less than the theoretical flame temperature. Direct measurements of this temperature could not be easily obtained. An approximate value for the chamber gas temperature was deduced from chamber pressure and propellant massflow measurements. This temperature was used for calculating the test section properties.

The gas viscosity and thermal conductivity in the test section were calculated using the method given in Reference 10. Since the products of combustion consist almost entirely of nitrogen and water vapor, the viscosity and the thermal conductivity were calculated considering these two components only.

The experimental values of the test section Mach number and gas specific heat ratio were obtained from pressure measurements taken across oblique and normal shocks of various intensities. Oblique and normal shocks in tandem arrangement were obtained with a combined wedge-pitot probe. As seen in Figure 19 an oblique shock is produced at the leading edge of the probe and a normal shock at the pitot probe. Variation of attitude of the probe permitted establishment of shocks of various intensities. The free stream Mach number and gas specific heat ratio were determined by comparing experimental and theoretical pressures for a number of different probe attitudes as shown in Figure 19. It should be noted that, because of the presence of a boundary layer on the probe, the experimental pressures, particularly at lower angles of deflection, are expected to be slightly higher than the theoretical pressures.

REFERENCES

1. P.S. Yip: Test Report for Phase I of the Aerodynamics Heating Tests at the NASA Langley Unitary Plan Wind Tunnel. Convair-Astronautics RT No. ZT-7-020 TN, August 1958.

2. P.S. Yip: Test Report for Phase II of the Aerodynamics Heating Tests at the Langley Unitary Plan Wind Tunnel. Convair-Astronautics RT No. ZT-7-025 TN, May 1959.

3. P.S. Yip: Test Report for Phase III of the Aerodynamics Heating Tests at the Langley Unitary Plan Wind Tunnel. Convair-Astronautics RT No. RT-7-027.

4. P.S. Yip: Test Report for Phase IV of the Aerodynamics Heating Tests at the Langley Unitary Plan Wind Tunnel. Convair-Astronautics RT No. AE-60-0175.

5. M.H. Bloom and A. Pallone: Heat Transfer to Surfaces in the Neighborhood of Protuberances in Hypersonic Flow. WADC TN 57-95.

6. R.J. Wisnieswki: Turbulent Heat-Transfer Coefficients in the Vicinity of Surface Protuberances: NASA Memo 10-1-58E, October 1958.

7. P.B. Burbank and H.K. Strass: Heat Transfer to Surfaces and Protuberances in a Supersonic Turbulent Boundary Layer. NASA RM L58E01A, July 1958.

8. E.R.G. Eckert: Engineering Relations for Heat Transfer and Friction in High-Velocity Laminar and Turbulent Boundary Layer Flow over Surfaces with Constant Pressure and Temperature. Transactions of the ASME, August 1956, pp 1273-1283.

9. M.L. Streiff: Heat Transfer to a Cone Segment Model. Convair-Astronautics ERR-AN-017, July 1960.

10. E. Kennard: Kinetic Theory of Gases. McGraw-Hill Co., 1938.

Distribution:

Astro	W.F. Radcliffe/W.B. Mitchell	595-10
	E.W. Schwartz	595-10
	G.O. Wilson	595-10
	Leo Berger	595-10
	R.S. Sherey	597-30
	D.R. Collins	541-10
	M.L. Streiff	595-10
	John Vasiliu	595-10
	Phil Yip	595-10
	R.E. Geisert	592-10
	Astro Library	521-30
San Diego	C.W. Frick	6-103
	F.A. Stephenson/J.W. Anderson	6-104
	R.F. Rolsten	6-181
	Eng. Library	6-157
	Thermo Lab File "D"	
	F.F. Leo	
	F.F. Baltakis (5)	

TABLE I

TEST SECTION FLOW PROPERTIES

	CALCULATED	MEASURED
Mach number	6.3	6.5
Velocity, ft/sec	8450	
Reynolds number, ft^{-1}	3.35×10^5	
Specific heat ratio	1.37	1.33
Total temperature, °R	4440	4350
Static temperature, °R	640	
Static pressure, psia		0.105

TABLE II

COMPOSITION AND PROPERTIES OF H_2 - AIR COMBUSTION PRODUCTS

AT STOICHIOMETRIC MIXTURE RATIO

MOLECULAR SPECIES	MOLE PERCENT
H_2O	33.65
N_2	64.84
H_2	0.721
O_2	0.218
OH	0.298
NO	0.216
H	0.033
O	0.0225
N	0.0000

Chamber pressure, psia	465
Total temperature, °R	4440
Total enthalpy, BTU/lb	1580
Molecular weight	24.42

TABLE III

FLAT PLATE HEAT TRANSFER RATES AND MAXIMUM SURFACE TEMPERATURES

T.C.	q $\frac{BTU}{ft^2-sec}$	T_2 °F	T.C.	q $\frac{BTU}{ft^2-sec}$	T_2 °F	T.C.	q $\frac{BTU}{ft^2-sec}$	T_2 °F
1	4.60	183	31	4.60	140	82	4.48	161
2	4.41	176	41	3.63	123	42	3.51	148
3	3.99	168	51	3.39	120	52	3.15	144
3A	3.80	157	61	3.14	115	62	2.91	141
4	3.56	152	71	2.90	115	72	2.66	137
4A	3.51	147	81	2.90	114	82	2.54	137
5	3.39	147	91	2.90	115	92	2.30	135
5A	3.15	141	101	2.90	117	102	2.18	135
6	3.15	141	111	2.90	120	112	2.18	136
6A	3.07	141	121	2.90	122	122	2.18	140
7	3.02	141	131	2.90	122	132	1.94	144
7A	2.95	144	141	2.90	120	142	1.94	150
8	2.83	145	151	2.90	120	152	1.94	154
10	2.66	142				162	1.69	144
11	2.42	141				172	1.69	146
12	2.42	143				182	1.94	147
13	2.42	145						
14	2.42	148						
15	2.18	151						
16	2.66	154						
17	2.42	158						
18	2.18	167						
19	1.94	204						
20	1.69	268						

P_1 = 0.18 psia

P_2 = 0.15 psia

P_3 = 0.43 psia

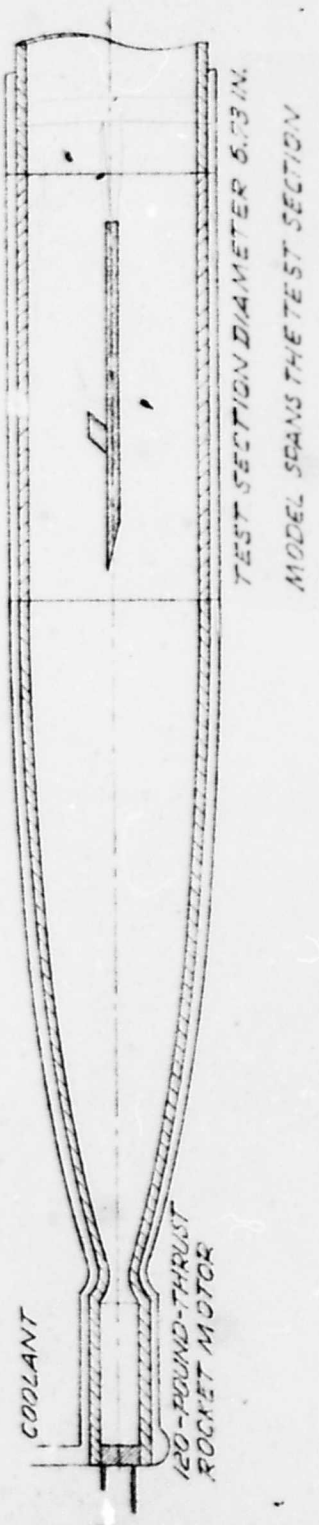

Fig. 1 - Experimental setup

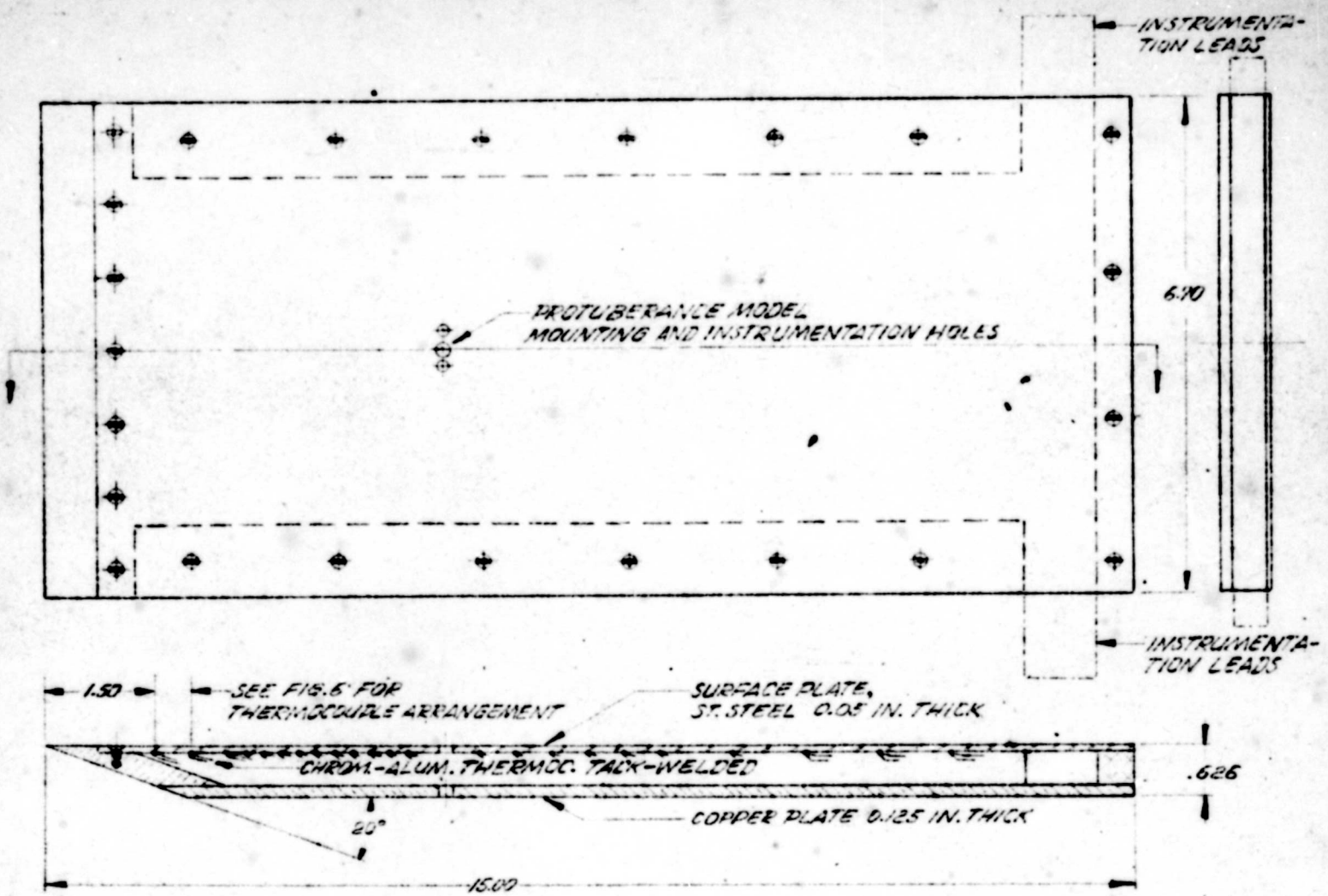

Fig. 2 - Heat transfer plate

Fig. 3 - Instrumentation and nesting of cylindrical pressure cells

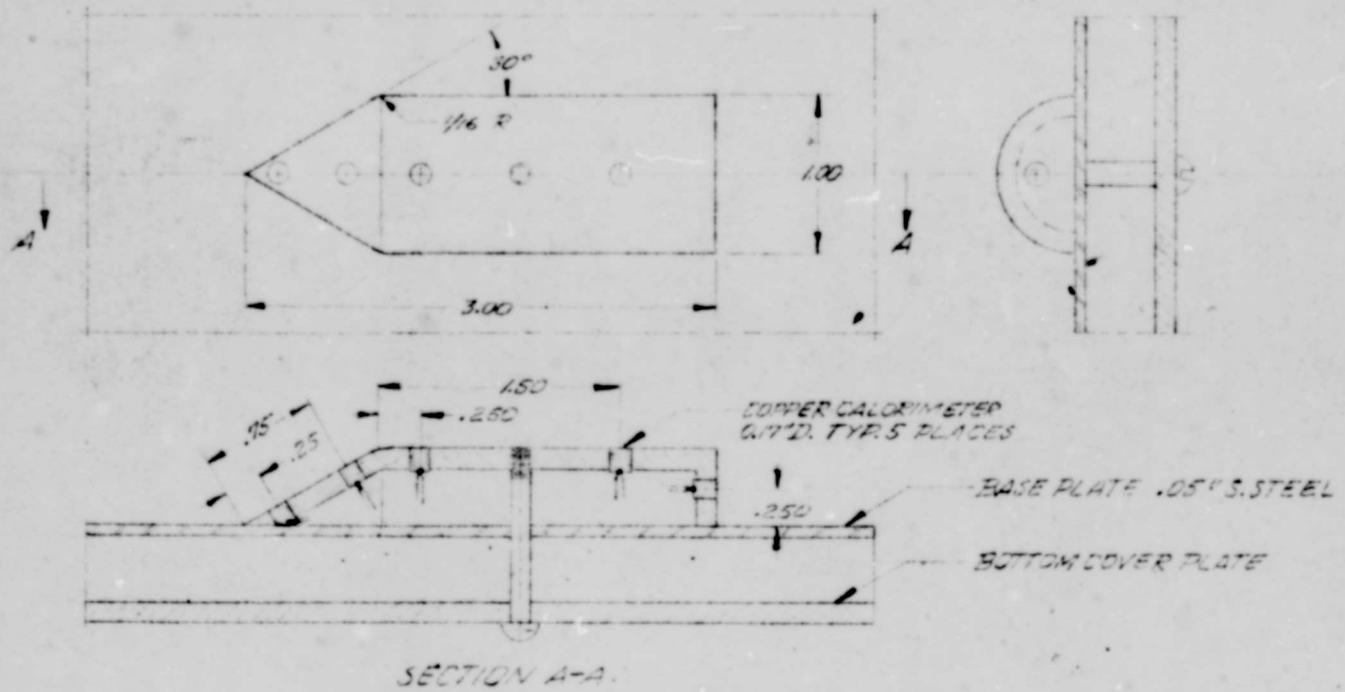

Fig. 4 - Instrumentation and mounting of semi-cone-afterbody protuberance model

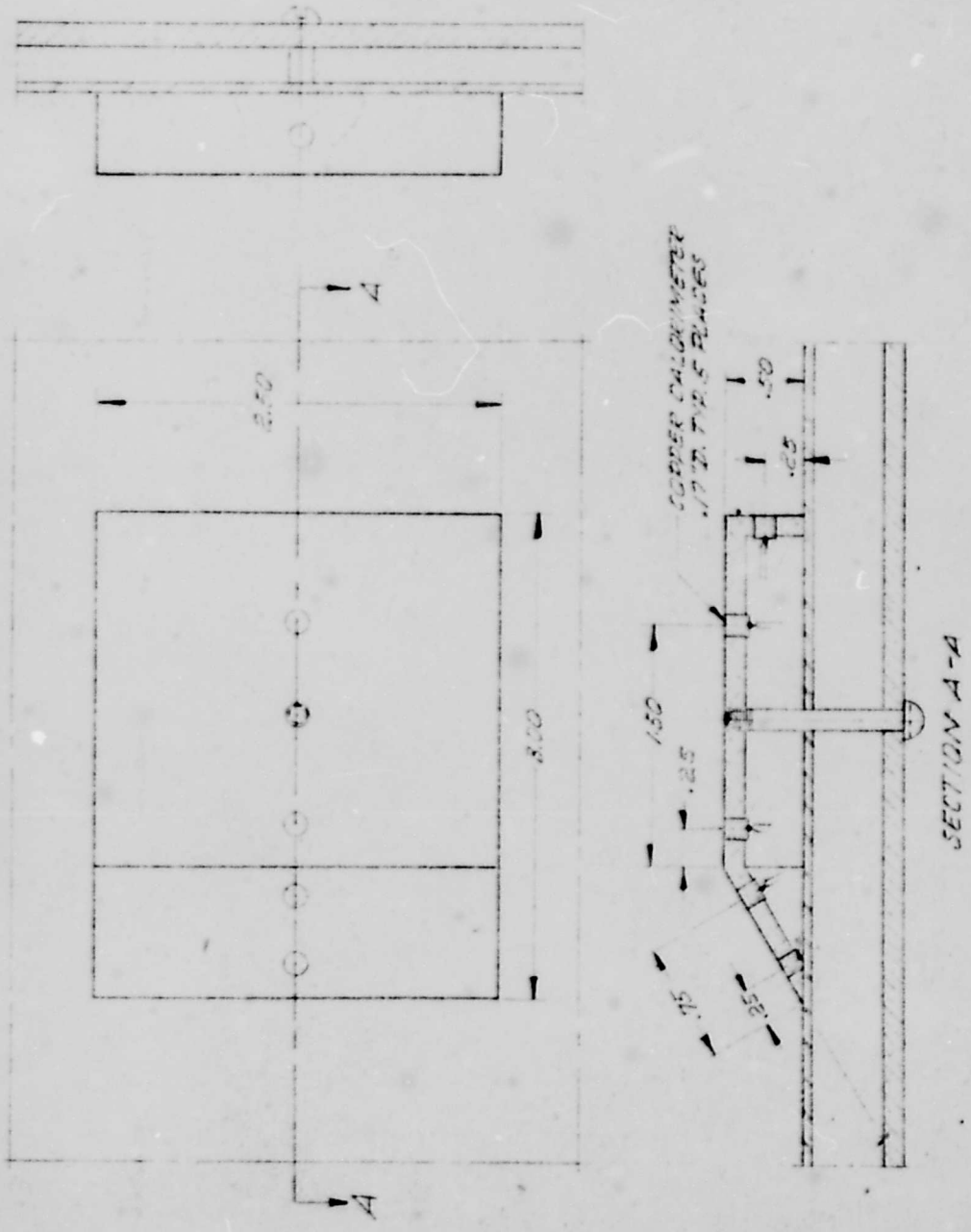

Fig. 5 - Instrumentation and mounting of wedge-afterbody protuberance model

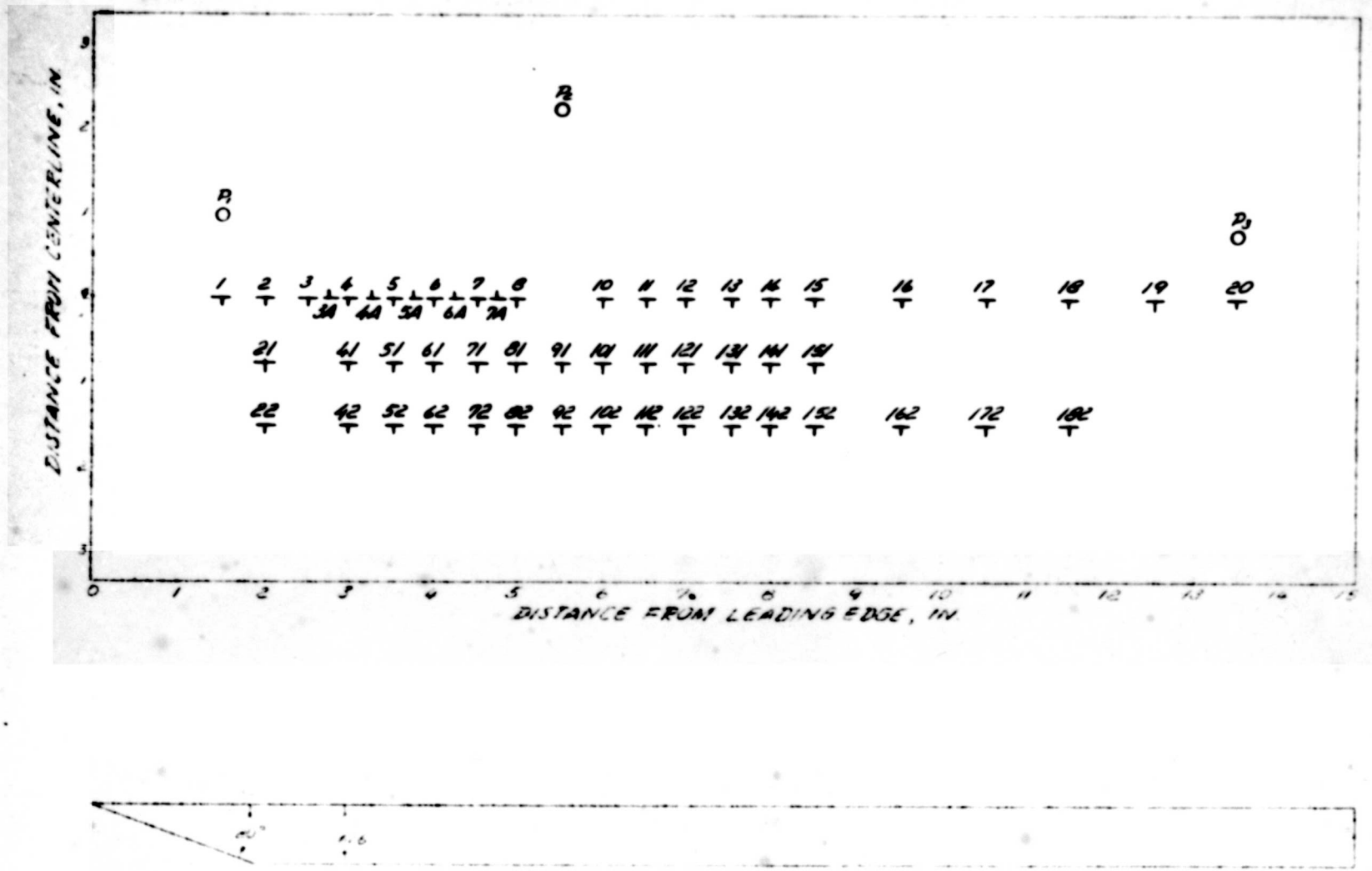

Fig. 6 - Thermocouple and pressure-orifice arrangement on the base plate

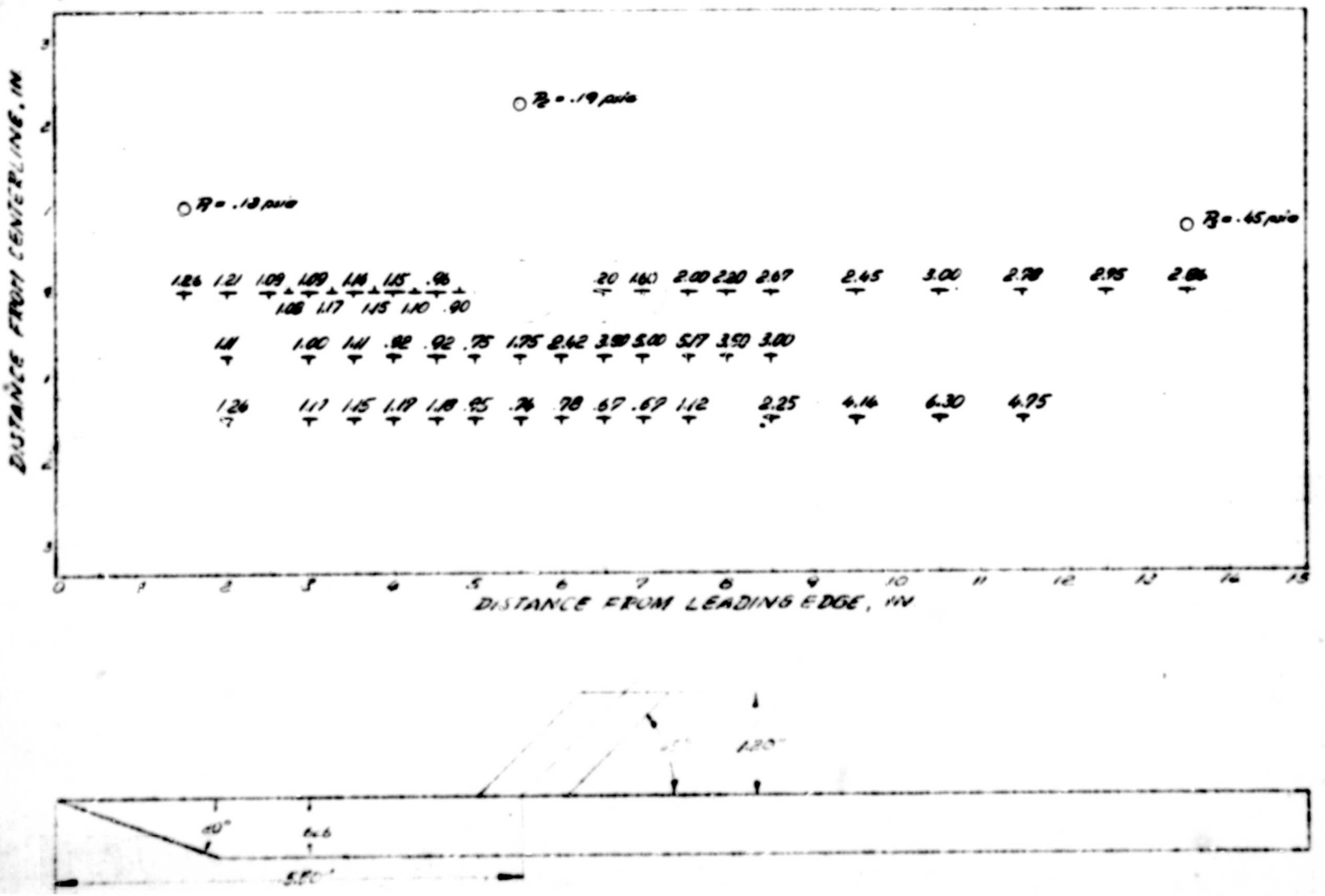

Fig. 7 - Ratios of local disturbed to undisturbed heating rates in the vicinity of a 3/4-inch diameter cylindrical protuberance

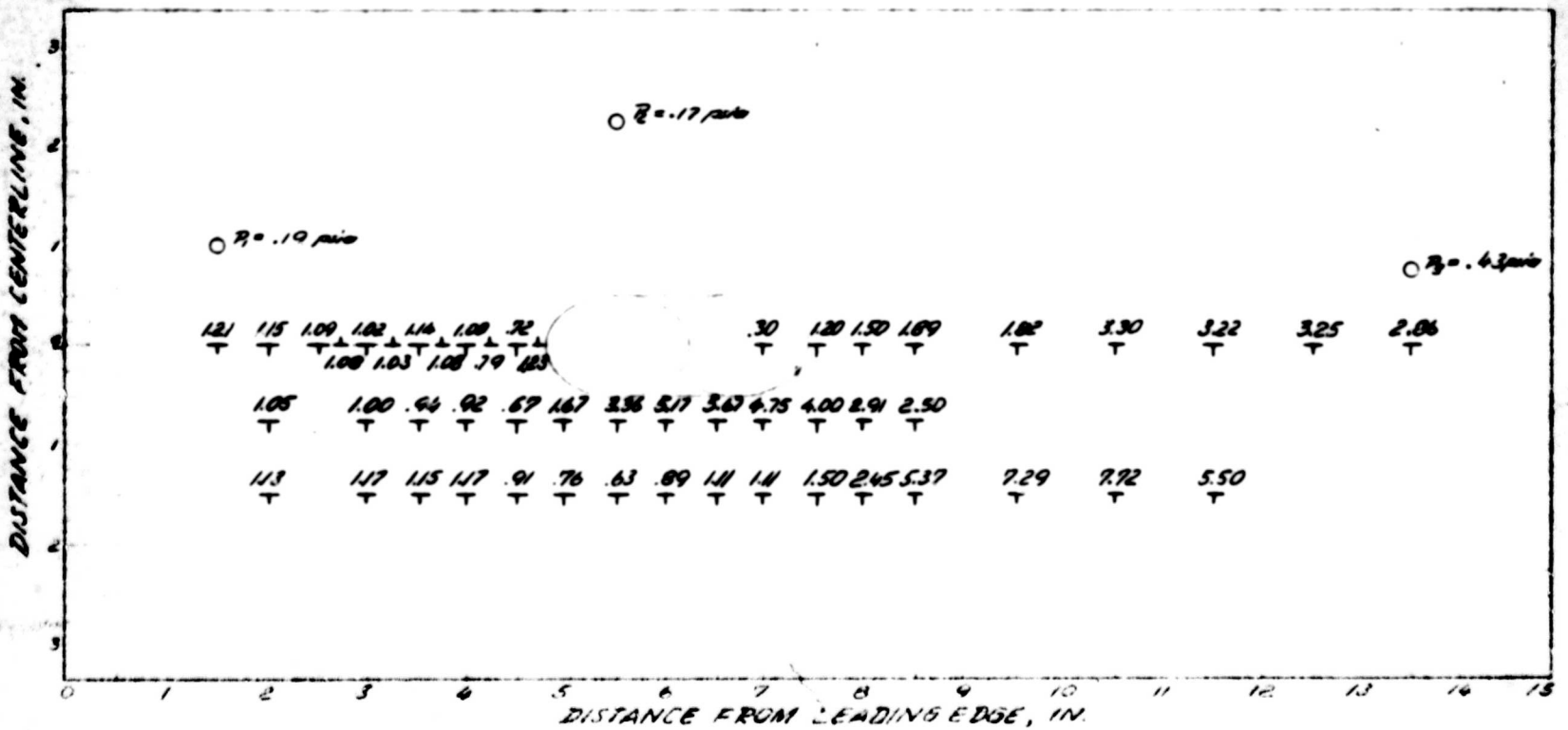

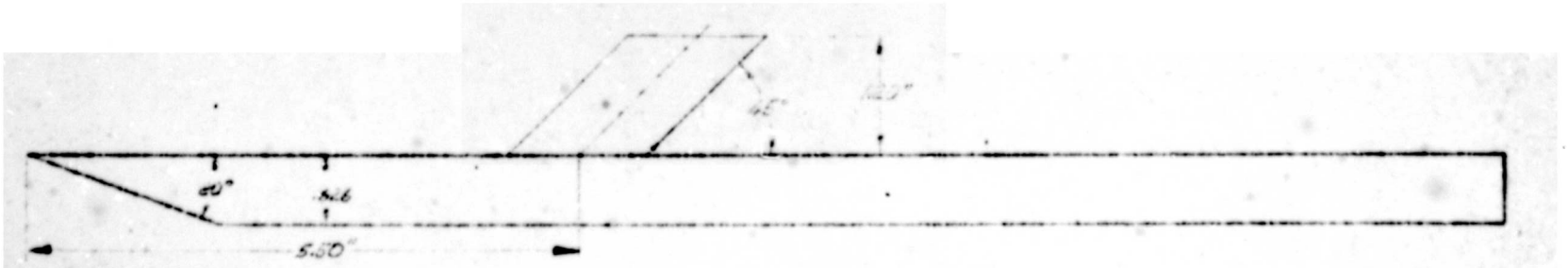

Fig. 8 - Ratios of local disturbed to undisturbed heating rates in the vicinity of a 1-inch diameter cylindrical protuberance

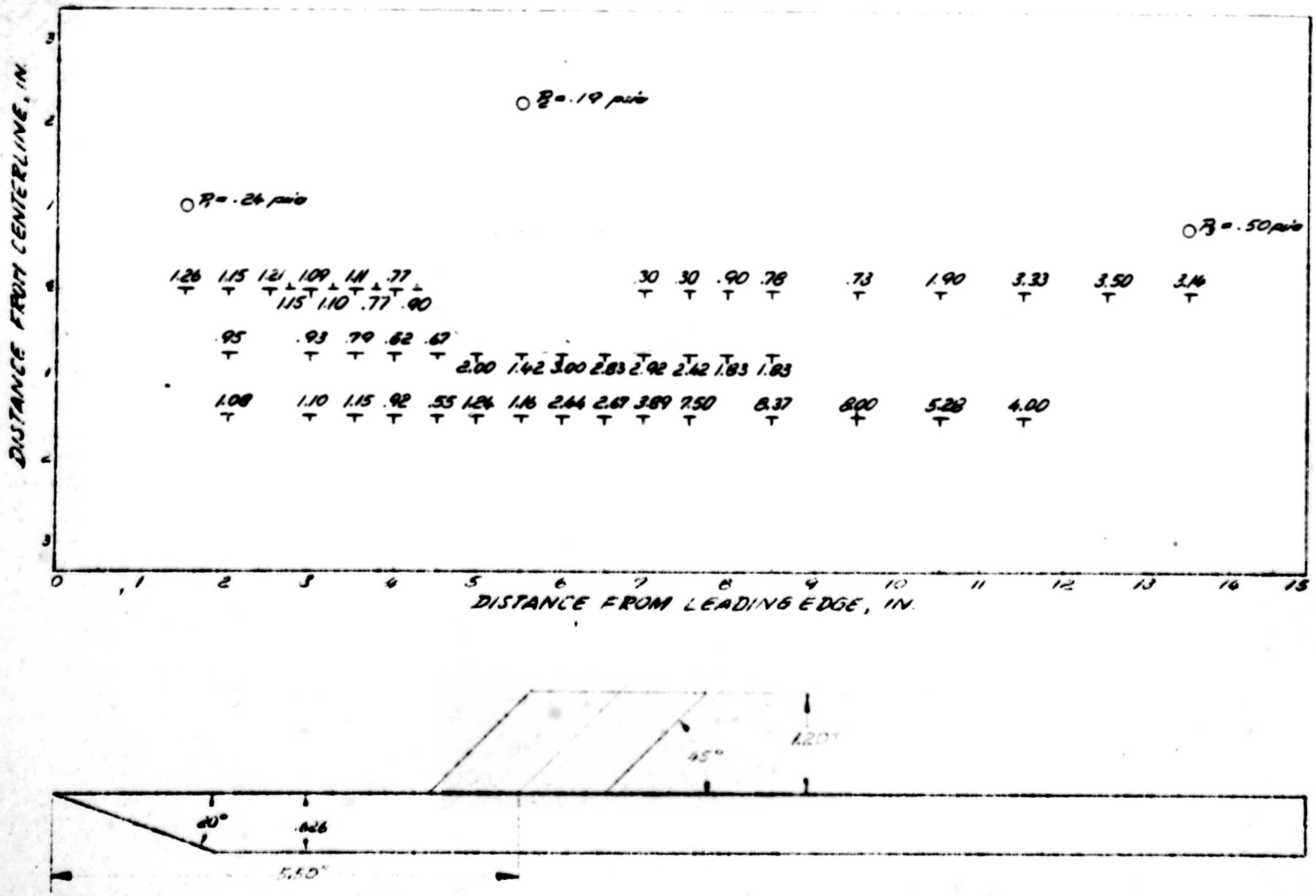

Fig. 9 - Ratios of local disturbed to undisturbed heating rates in the vicinity of a 1.5-inch diameter cylindrical protuberance

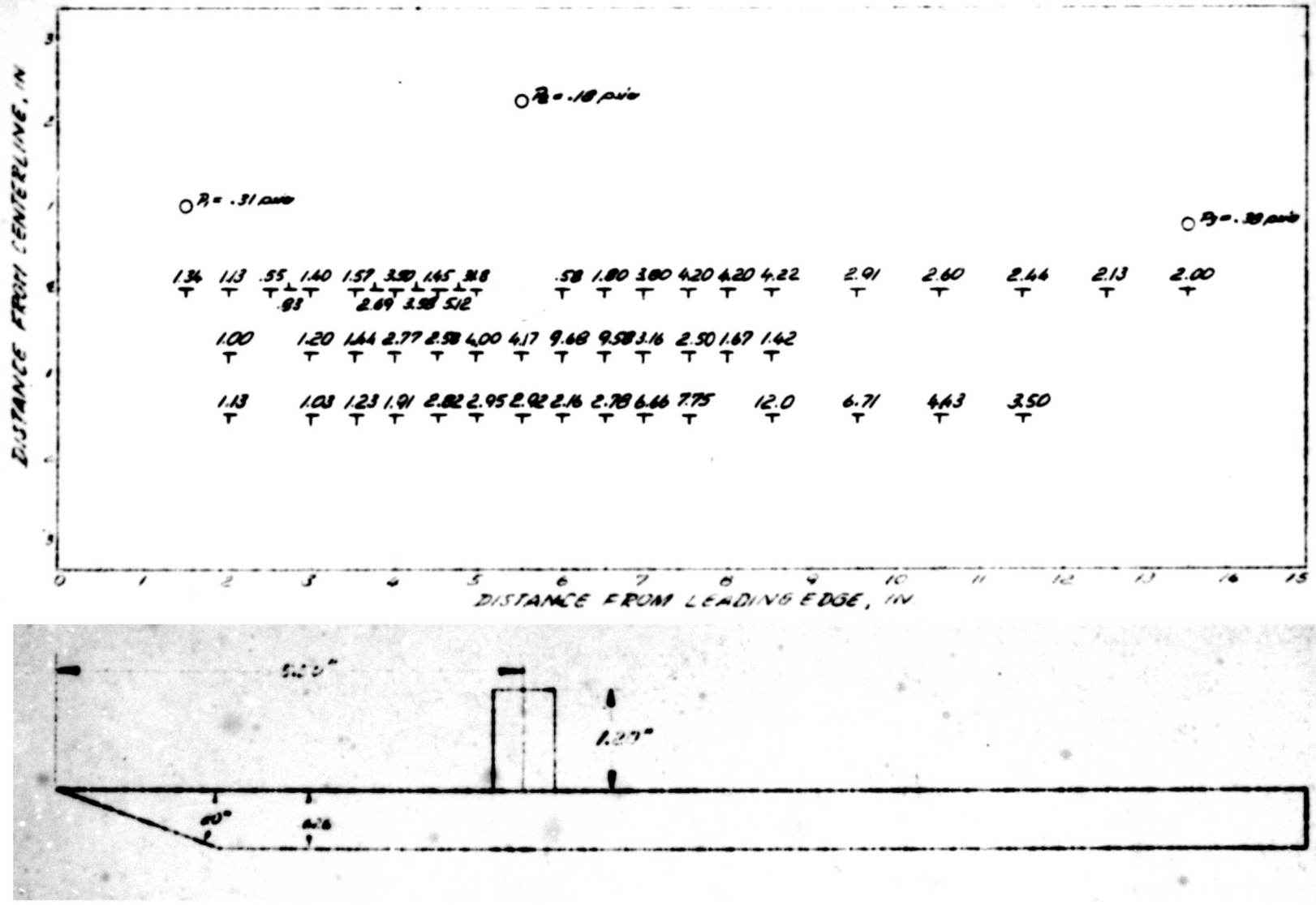

Fig. 10 - Ratios of local disturbed to undisturbed heating rates in the vicinity of a 3/4-inch diameter cylindrical protuberance

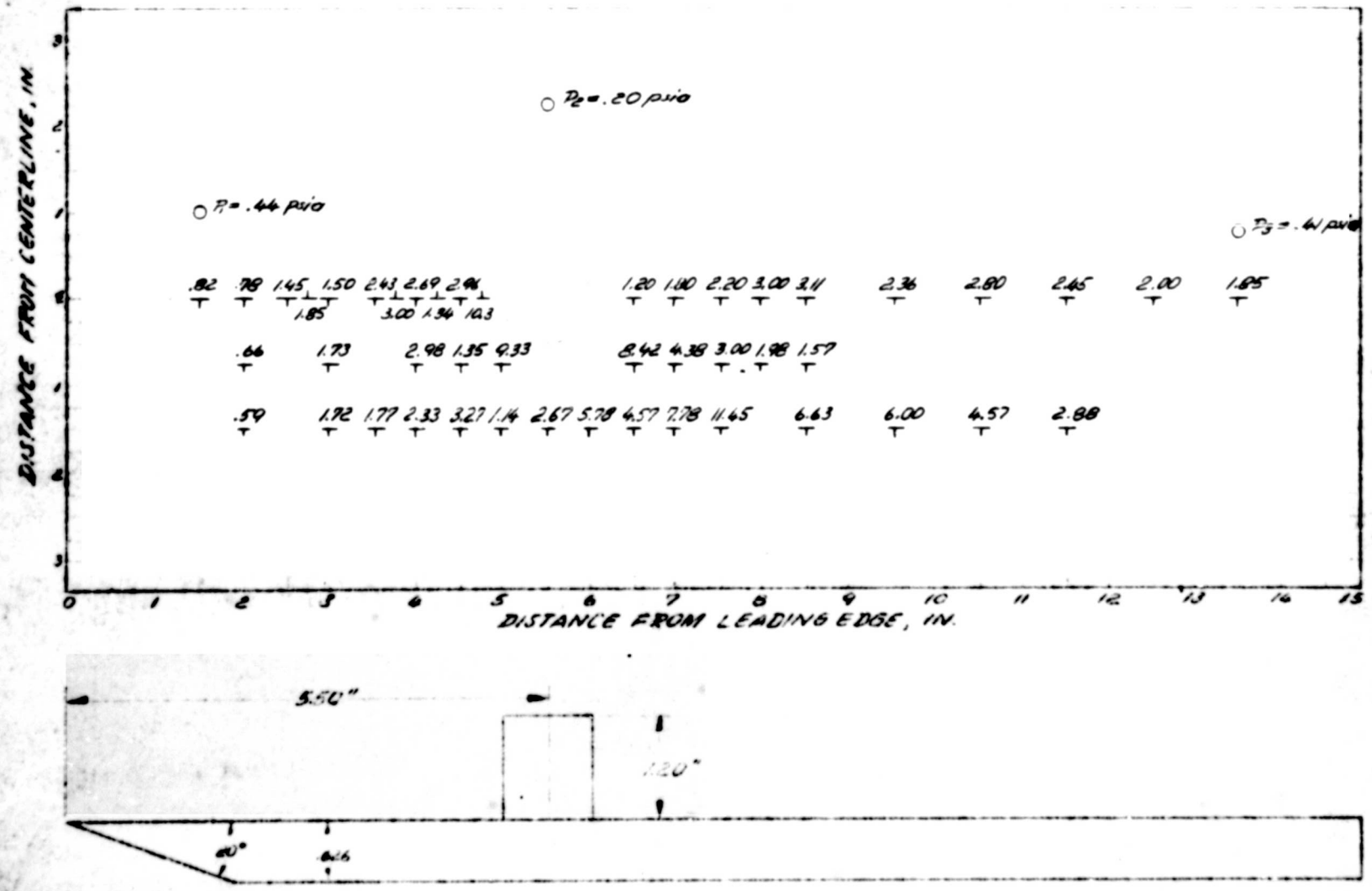

Fig. 11 - Ratios of local disturbed to undisturbed heating rates in the vicinity of a 1-inch diameter cylindrical protuberance

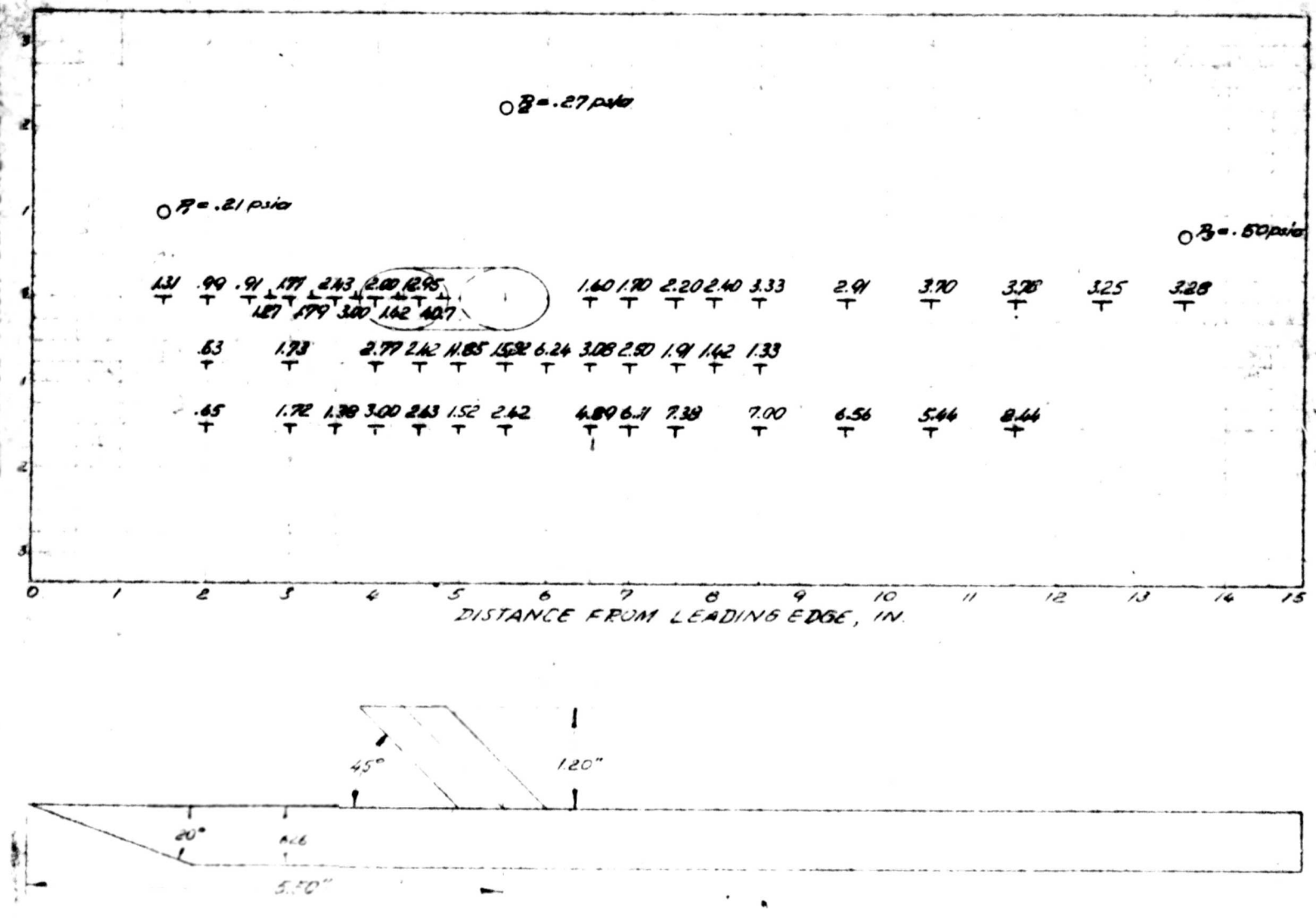

Fig. 12 - Ratios of local disturbed to undisturbed heating rates in the vicinity of a 3/4-inch diameter cylindrical protuberance

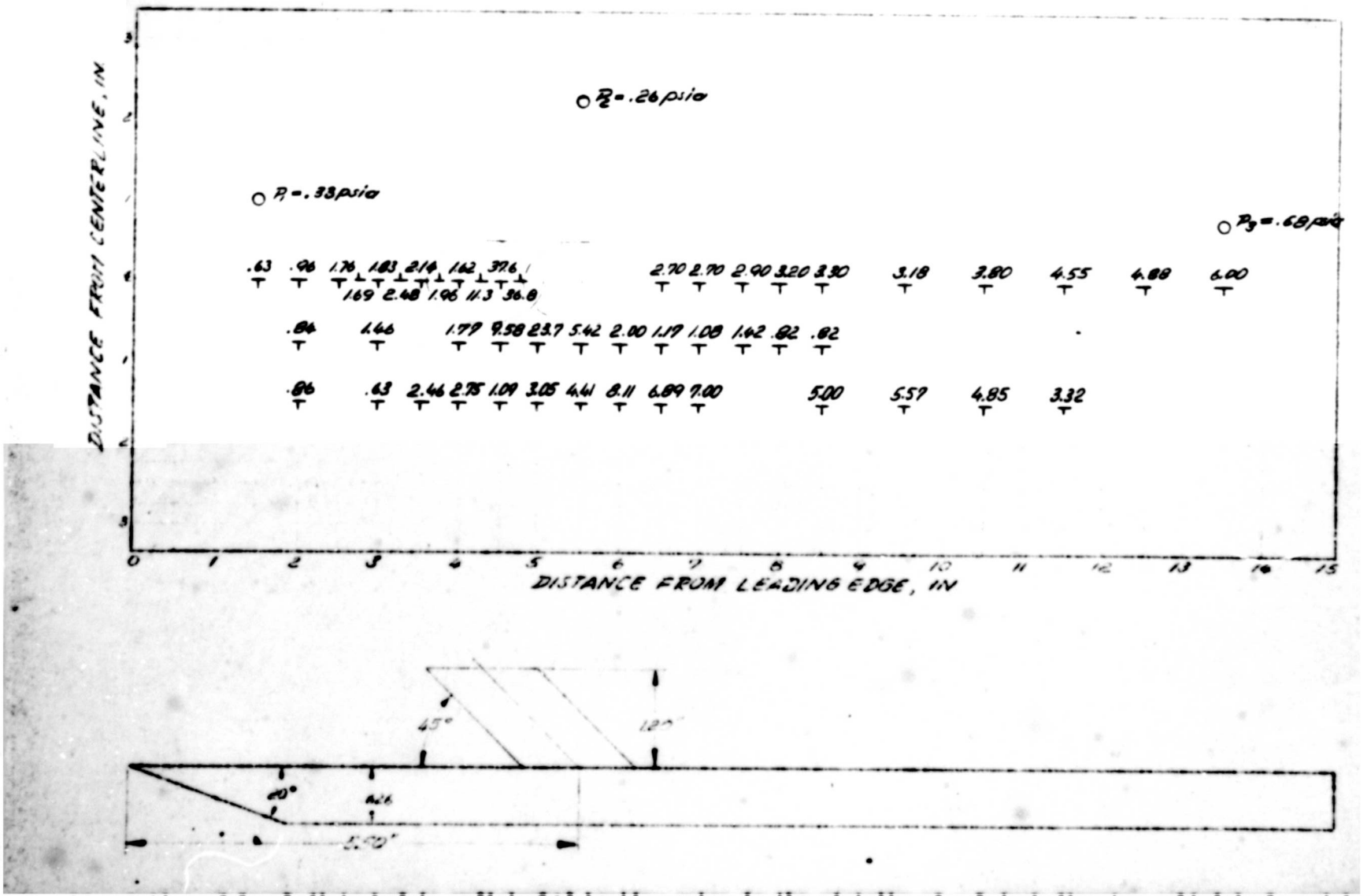

Fig. 13 - Ratios of local disturbed to undisturbed heating rates in the vicinity of a 1-inch diameter cylindrical protuberance

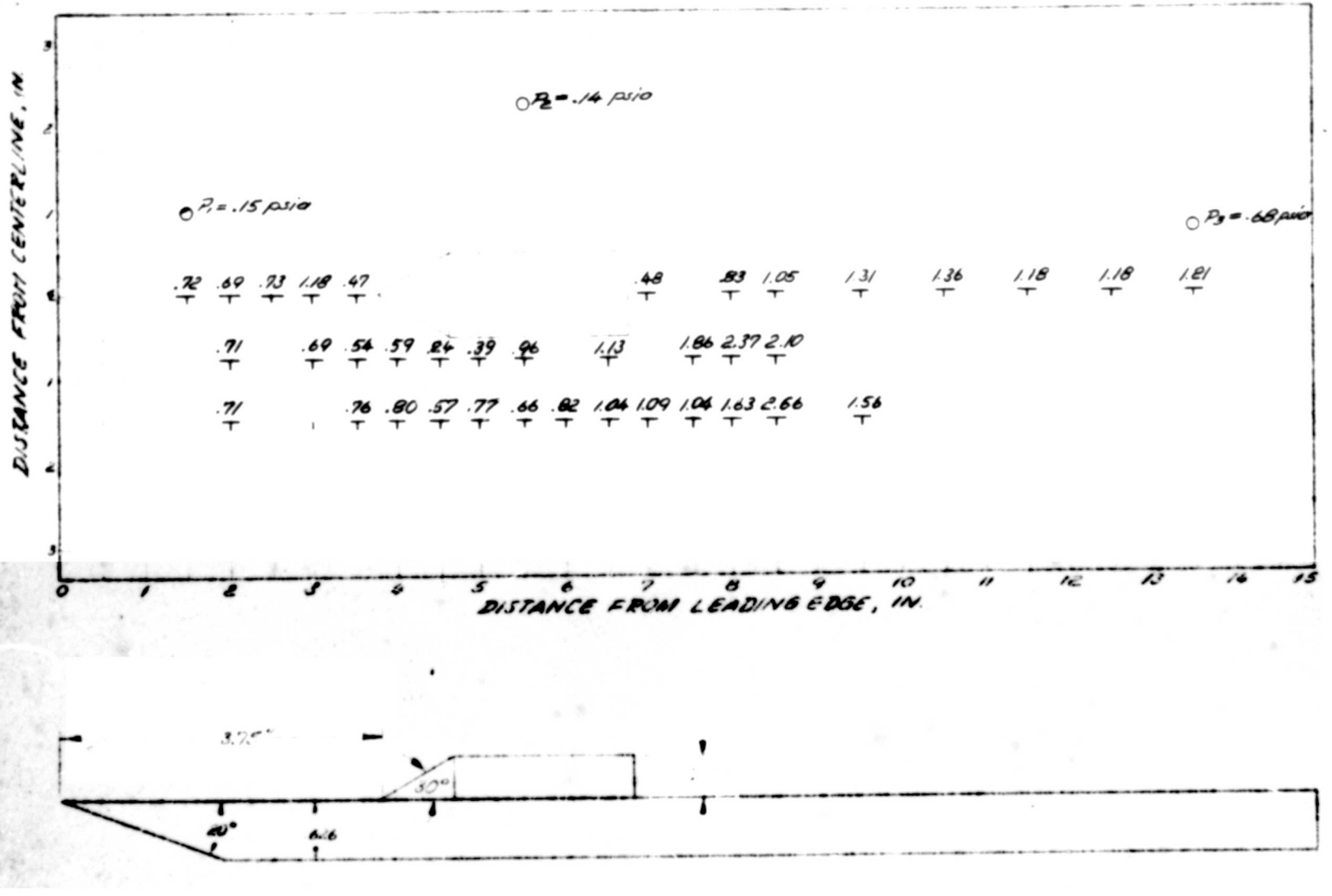

Fig. 14 - Ratios of local disturbed to undisturbed heating rates in the vicinity of a semi-cone-afterbody protuberance

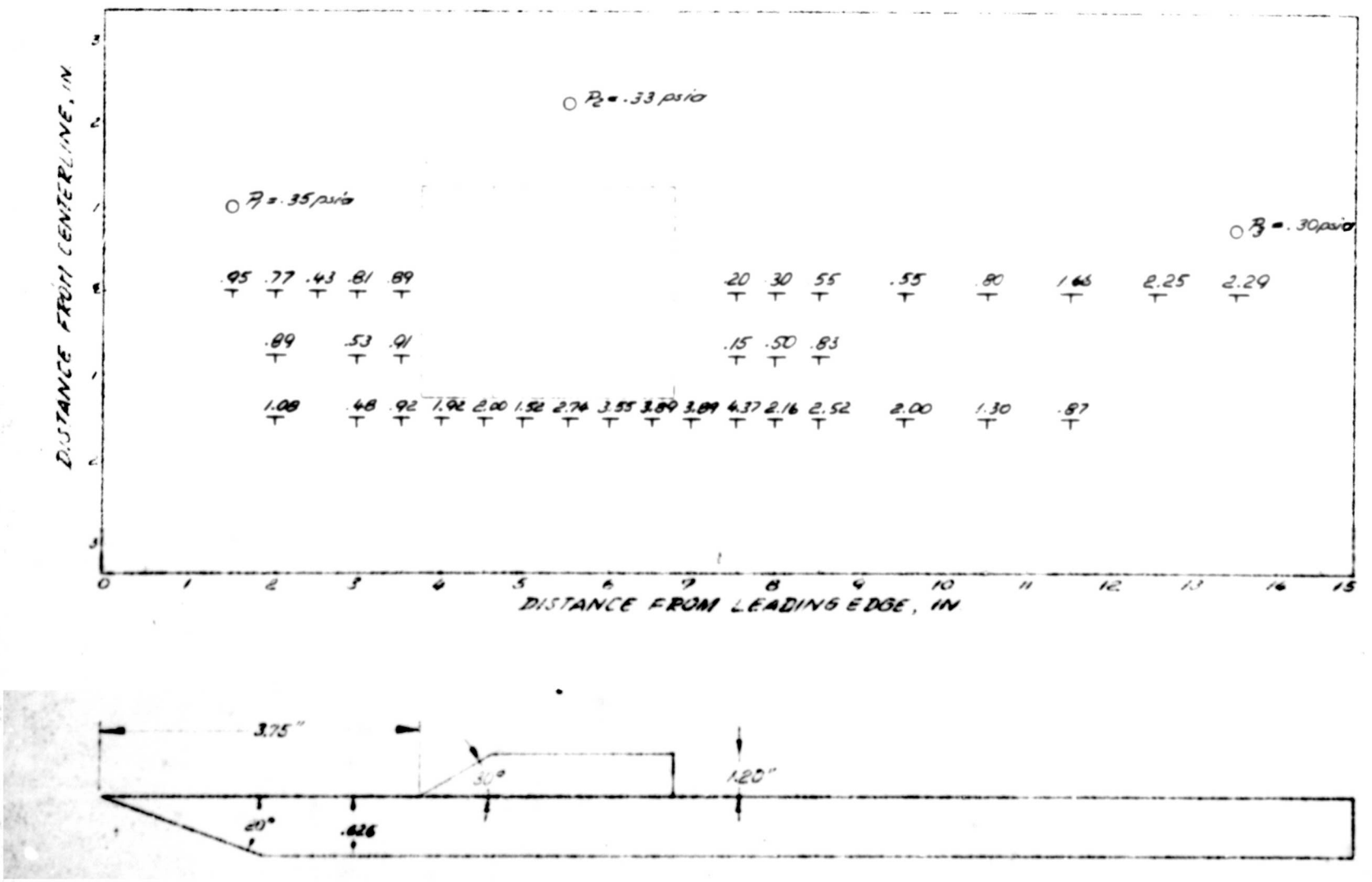

Fig. 15 - Ratios of local disturbed to undisturbed heating rates in the vicinity of a wedge-afterbody protuberance

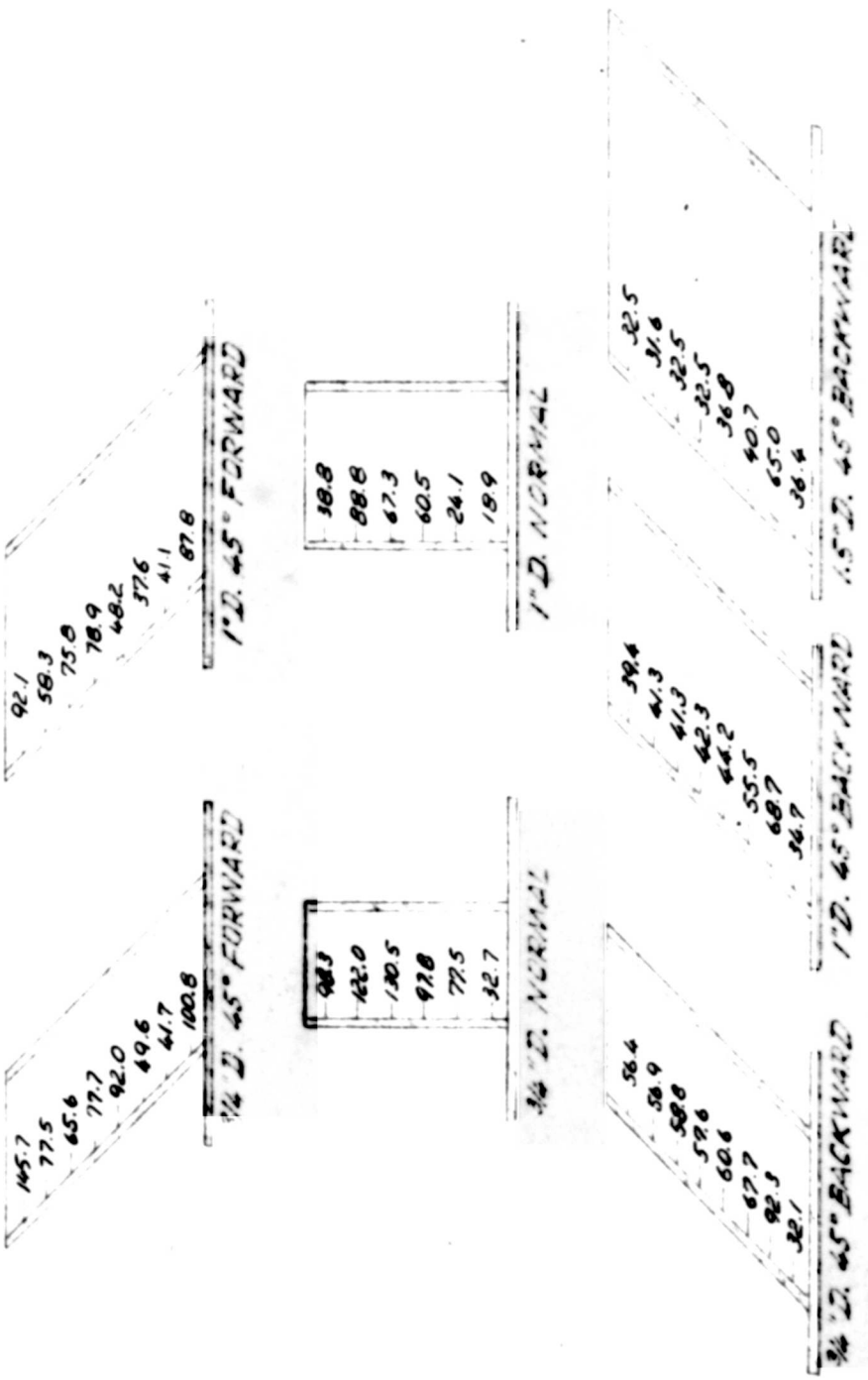

Fig. 16 - Heat transfer rates on cylindrical protuberance models, BTU/ft²-sec

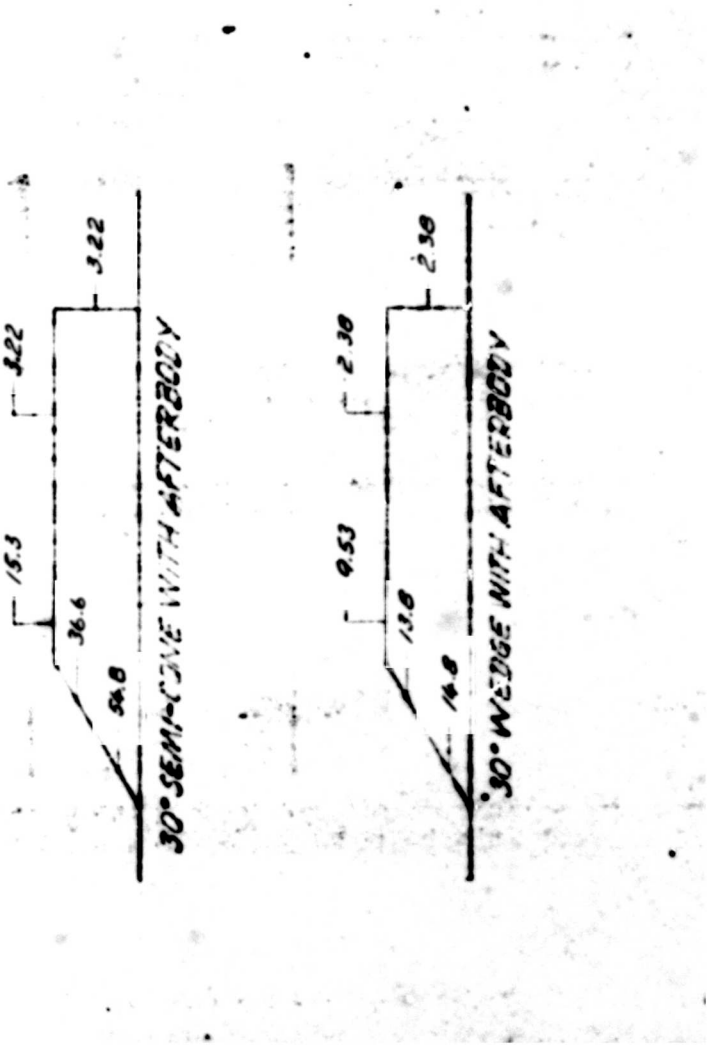

Fig. 17 - Heat transfer rates on semi-cone and wedge-cylinder pressurance models, BTU/ft²-sec

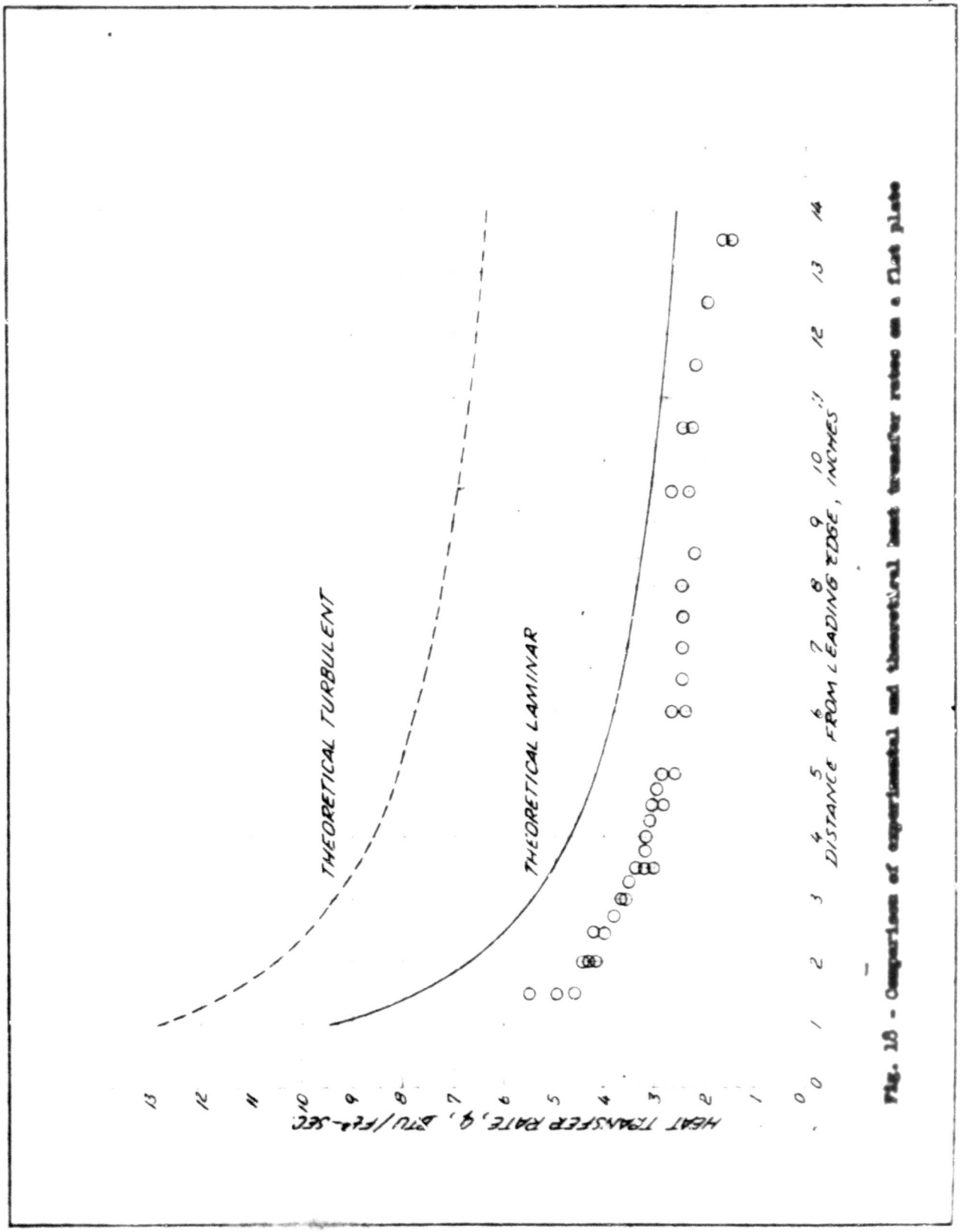

Fig. 10 - Comparison of experimental and theoretical heat transfer rates on a flat plate

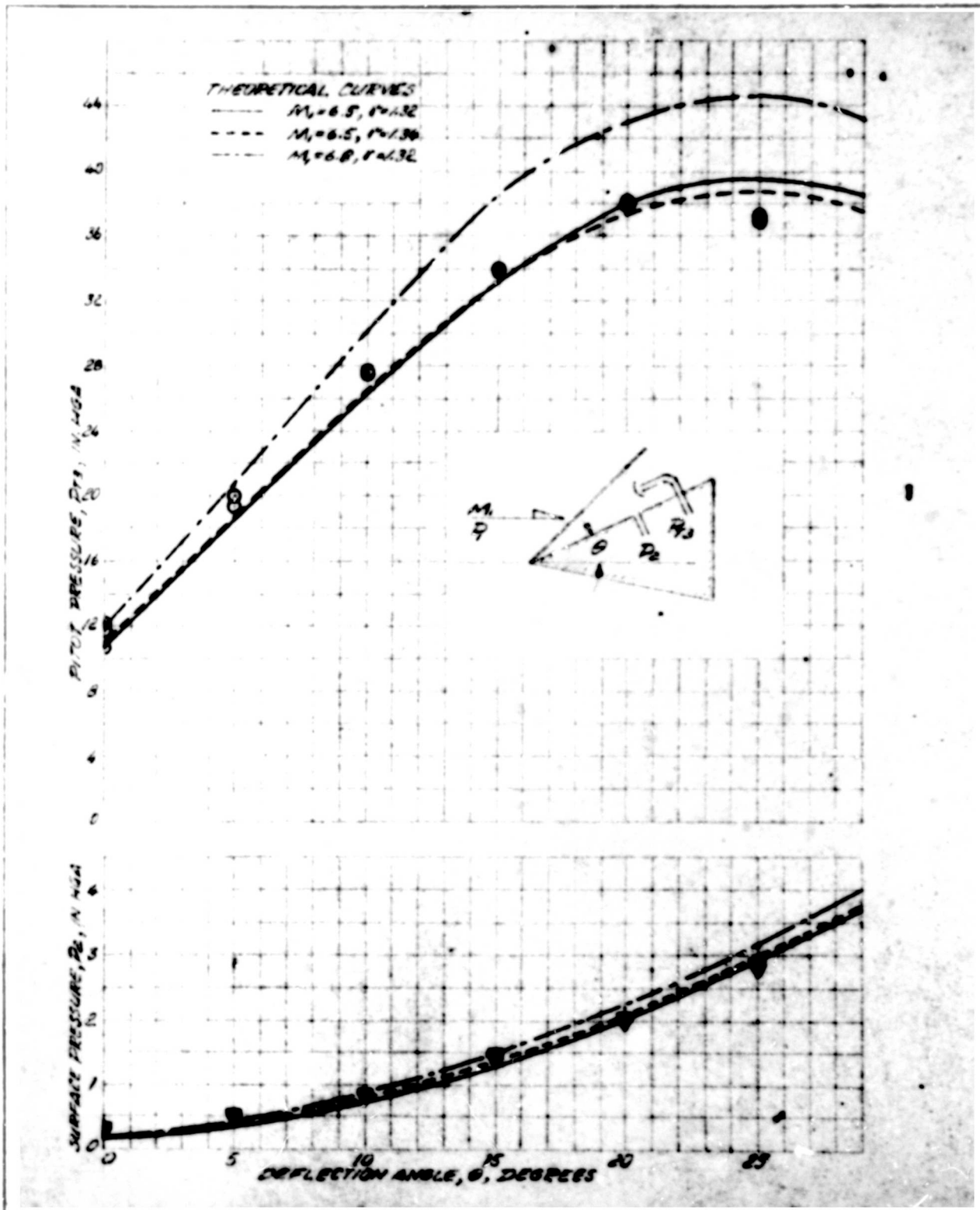

Fig. 19 - Comparison of experimental and theoretical calibration pressure data